WILEY-VCH

Sheet-Based Fluidic Diodes for Embedded Fluidic Circuitry in Soft Devices

*Vi T. Vo, Anoop Rajappan, Barclay Jumet, Marquise D. Bell, Sofia Urbina, Daniel J. Preston**

V. T. Vo, Dr. A. Rajappan, B. Jumet, M. D. Bell, S. Urbina, Prof. D. J. Preston

Department of Mechanical Engineering, Rice University, Houston, TX 77005, USA

*Email: djp@rice.edu

Keywords: fluidic circuits, pneumatic actuators, soft robotics, digital logic, analog control

Abstract

The recent development of soft fluidic analogs to electrical components aims to reduce the demand for rigid and bulky electromechanical valves and hard electronic controllers within soft robots. Here, we advance this ongoing effort by creating sheet-based fluidic diodes constructed from readily available flexible sheets of polymers and textiles using a layered fabrication approach amenable to manufacturing at scale. These sheet-based fluidic diodes restrict reverse flow over a wide range of differential pressures—exhibiting a diodicity (the ratio of resistance to reverse versus forward flow) of approximately 100x—to address functional limitations exhibited by prior soft fluidic diodes. By harnessing our diode's highly unidirectional flow, we realize soft devices capable of (i) facilitating the capture and storage of pressurized fluid, (ii) performing Boolean operations using diode logic, (iii) enabling binary encoding of circuits by preventing interactions between different pressurized input lines, and (iv) converting oscillating input pressures to a direct current–like, positively phased output. This work exemplifies the use of fluidic diodes to achieve complex patterns of actuation and unique capabilities through embedded fluidic circuitry, enabling future development of sheet-based systems—including wearable and assistive robots made from textiles—as well as other soft robotic devices.

1. Introduction

Pressure-driven soft robots have emerged as a promising approach to enable the complex interactions required in unstructured and dynamic environments.[1–7] These robots often utilize integrated, flexible actuators controlled by the inflation and deflation of internal channels or bladders with pressurized fluid,[8–11] resulting in deformable structures useful for tasks requiring adaptability and compliance. The internal pressure of these structures can be varied to achieve complex and adaptive motions through nonlinear deformations that can be difficult to achieve with rigid components.[7,12–14] The practical implementation of these pneumatic soft robots, however, still faces two main challenges: (i) the demand for a number of control signal inputs that increases proportionally with the number of independent soft actuators due to a lack of embedded control;[13–16] and (ii) the reliance on rigid and bulky electronic control systems and hard electromechanical valves, resulting in increased complexity (i.e., interfacing electrical and fluidic systems) and weight while limiting deformability. [14,16–20]

Fluidic computing, or the manipulation of pressurized fluids to perform computational tasks, introduces an alternative approach enabling electronics-free control systems for pneumatic soft robots. Instead of relying on traditional electronic components, fluidic logic gates and circuits can be embedded within a robot's structure to program sequential actions and control its movement in response to stimuli. While microfluidic devices have shown potential in achieving precise and intricate control in applications such as lab-on-a-chip and bioinspired microrobotics, these systems are often not practical for mesoscale robotics applications due to challenges in scaling that arise due to (i) pressure requirements (smaller fluidic channels require greater pressures to drive fluid flow or remain limited to lower flow rates), (ii) fabrication processes (microfluidic processes typically use soft lithographic approaches that may not translate to the mesoscale easily), and (iii) material compatibility (microfluidic systems have typically included glass or silicon, which compromise a soft construction).[21–29]

Alternatively, recently developed mesoscale soft fluidic circuits use compliant materials to create devices for robotic control, with individual components documented in prior work successfully demonstrating functionalities analogous to electronic counterparts.[16,30–36] Among these soft fluidic components, soft fluidic diodes (i.e., one-way valves or check valves) are relatively unexplored despite their distinct functionality. Furthermore, existing soft fluidic diodes exhibit limitations including (i) bulky three-dimensional architectures, which impose functional limitations specifically for robots navigating in space-constricted or resource-constrained environments,[37–40] and (ii) sub-optimal performance, primarily concerning the required closing pressure before fully restricting backflow.[18]

In this work, we created a sheet-based fluidic diode that passively restricts backflow by collapsing an internal channel **(Figure 1)**. Following a general trend in soft robotics toward implementation of flexible, sheet-based materials (e.g., acetate[30,41,42], paper[43–47], and textiles[31,48–50]) due to the lightweight and low-profile designs they enable, our sheet-based diode is composed of commercially available sheet materials including nylon taffeta with thermoplastic polyurethane (TPU) film that are assembled using a scalable process of thermal lamination. To understand the flow behavior of the diode and to guide future circuit design, we characterized the fluidic resistance (i.e., the relationship between the volumetric flow rate and the differential pressure across the diode) and developed a scaling law relating fluidic resistance to diode size. We also demonstrated functionalities enabled by our sheet-based diodes (**Figure 1**D) including: (i) capturing and storing pressurized air when coupled with pneumatic pouches (i.e., capacitors), as exemplified in practical applications of a self-sealing balloon and an inflatable car jack; (ii) making decisions with diodes arranged as logic gates that use levels of air pressure to perform computational logic; (iii) facilitating the routing of fluid along designated pathways, exemplified by a fluidic encoder generating binary indices;

and (iv) rectifying air flow by converting oscillating pressure inputs to a positive-phase, DC-like output pressure, demonstrated by integrating the diodes into a textile-based energy harvesting system can extract pneumatic energy from walking. These sheet-based fluidic diodes represent fundamental mechanofluidic computing elements that enable embedded, multifunctional circuits for programmable control of pneumatically actuated robots.

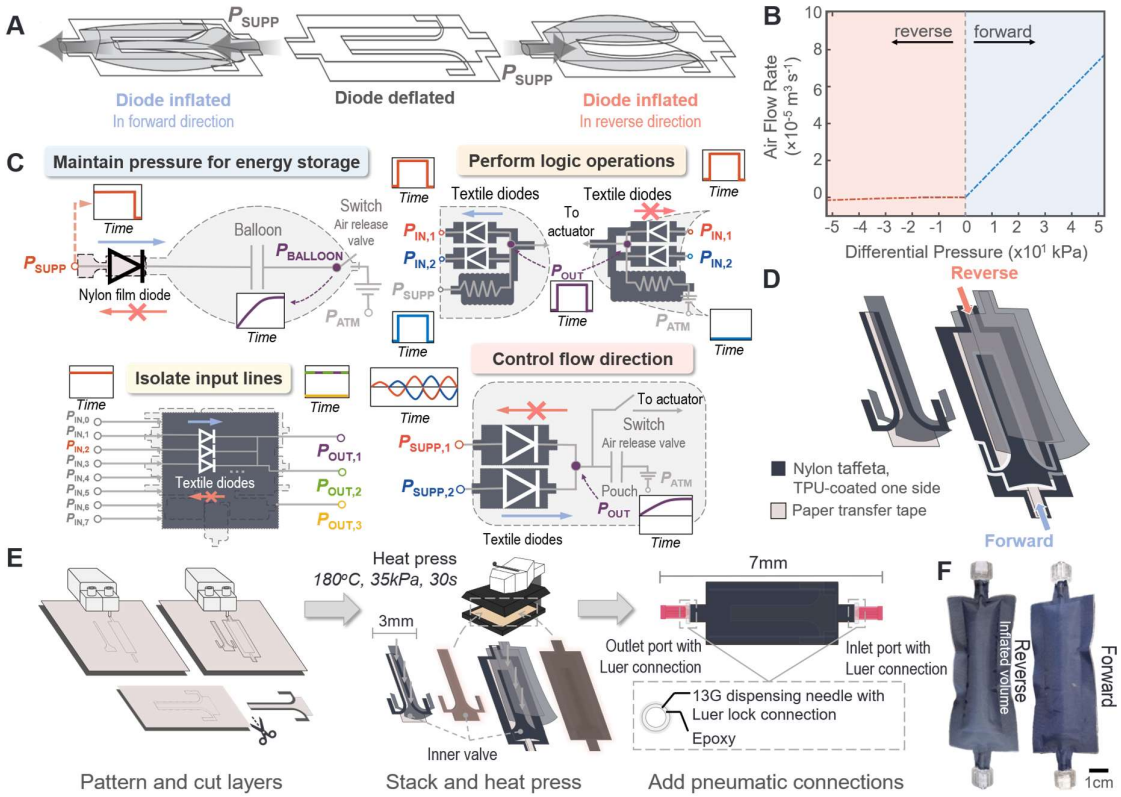

Figure 1. Sheet-based fluidic diode. (A) Operation of the diode: in the forward mode, air flows through the internal channel and exhausts at the outlet port; in the reverse mode, air fills the internal volume of the encasing pouch, resulting in a compressive force that pinches the internal channel closed and prevents air from flowing, even for vanishingly small pressure differences in the reverse flow direction because the requisite pressure drop corresponding to any level of flow through the internal channel would result in a lower pressure within the flow channel than in the surrounding pouch. (B) Representative behavior of the volumetric flow rate as it depends on differential pressure across the internal channel of the diode. The plot indicates forward and reverse modes consistent with the performance characteristics of electronic diodes. (C) Overview of the types of fluidic circuits constructed using sheet-based diodes to achieve various functionalities. (D) Internal layout and alignment of the sheet-based diode fabricated using textiles, illustrating the internal channels. (E) Fabrication process of the sheet-based diode. (F) Photographs of the sheet-based diode.

2. Results

2.1. Device Design and Characterization

Our sheet-based diode consists of two main functional features: (i) a duckbill-like channel connected to the inlet port that flows into (ii) an encasing chamber surrounding the channel. The operating principle of the diode draws inspiration from microfluidic pinch valves; as pressurized air accumulates inside the encasing chamber, it exerts a compressive force on the channel and pinches the walls together, sealing the valve against flow.[24] The design of the inner duckbill channel is critical; after testing various geometries and ratios of width to length, we found that the inner duckbill channel effectively restricts flow at an aspect ratio of 0.0974 ("1.00" scale has a width of 3.0mm and a length of ~30.8mm). Our work achieves flow polarity based on a two-dimensional architecture, differentiating it from previous designs of fluidic diodes that either use three-dimensional elastomeric materials (e.g., rubber flaps, O-rings, and elastic membranes)[18] or rely on rigid materials (e.g., acrylic or 3D-printed pieces) to form the physical barrier blocking flow.[38,39]

We then characterized the flow behavior of the fluidic diode by plotting the flow rate as a function of the differential pressure across the diode. From the experimental data, we observe two distinct operating regimes based on the polarity of the differential pressure, indicating that the fluidic diode exhibits performance analogous to that of an electronic diode. In the forward direction, increasing differential pressures result in linearly increasing flow rates (**Figure 2**). In the reverse direction, the flow rate remains near 0 m^3s^{-1} indicating not only the prevention of backflow but also the absence of a minimum pressure required to close the valve in the reverse flow, in contrast to some prior work in literature—a constraint that arises due to the geometry or material properties of the sealing mechanism responsible for restricting flow. To quantitatively determine the fluidic resistance across the valve, we modified the design of the device by adding two ports directly before the entrance and after the exit of the internal duckbill channel (**Figure 2**A), which allows measurement of differential pressure across the diode without accounting for the resistances of the fluidic connections. We found

that the diodicity (i.e., the ratio of flow resistances for reverse versus forward flow, which are inversely proportional to the slopes in Fig. 2C) was approximately 100x, indicating sufficient performance for most fluidic applications. Meanwhile, for forward flow, we determined that the fluidic resistance of the diode is inversely proportional to the lengthscale of the diode to the power of 3, following the expected isometric scaling relationship. The linear relationship observed from the lines in **Figure 2**B suggests that the flow across the internal channel is within the laminar regime. We observe slight deviations between the model curve and measured data as the lengthscale increases (**Figure 2**D), potentially indicating entry into the turbulent flow regime. The predictability of the diode's performance based on this analysis is limited to specified flow rates and lengthscales corresponding to laminar flow, although it could be extended to turbulent flow either empirically or through more detailed modeling.

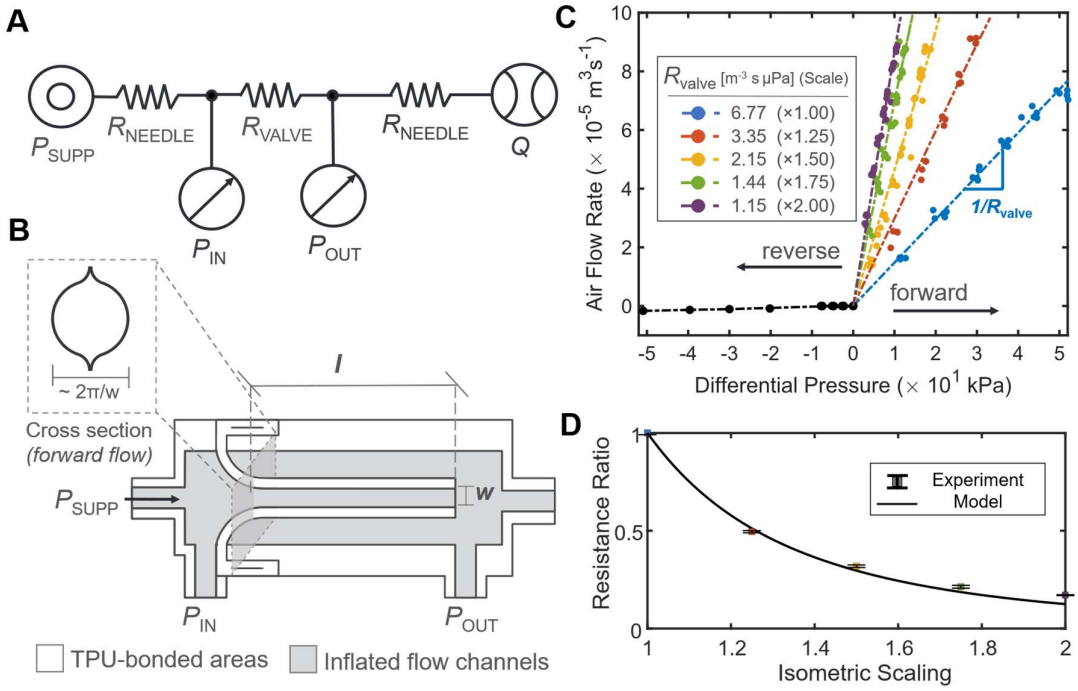

Figure 2. Schematics and experimental data showing the fluidic characteristics of our diode. (A) Circuit diagram representation of the pneumatic testbed for flow behavior of the sheet-based fluidic diode. (B) Cross-sectional view (inset) of the experimental testbed with ports to measure differential pressure across the diode, eliminating effects of the fluidic connections at the inlet and outlet. (C) Experimental results for fluid flow versus differential pressure for the fluidic diode. (D) Experimental data versus model prediction showing the effect of isometric scaling on the resistance ratio for forward flow (i.e., compared to the x1.00 scale).

2.2. Static Demonstrations

Fluidic diodes allow for energy storage when coupled with a pneumatic pouch or other known volume (i.e., a fluidic component analogous to an electronic capacitor). For a system subjected to a momentary or static fluidic input signal (e.g., a constant high-pressure input), this configuration facilitates the capture and storage of pressurized fluid by allowing fluid to enter and accumulate within the capacitor while limiting backflow of the fluid when the high-pressure source is removed, ensuring a stable pressurized environment with near-negligible deflation. We demonstrate the diode's capability for maintaining pressure through practical examples of a self-sealing balloon and an inflatable car jack (**Figure 3**).

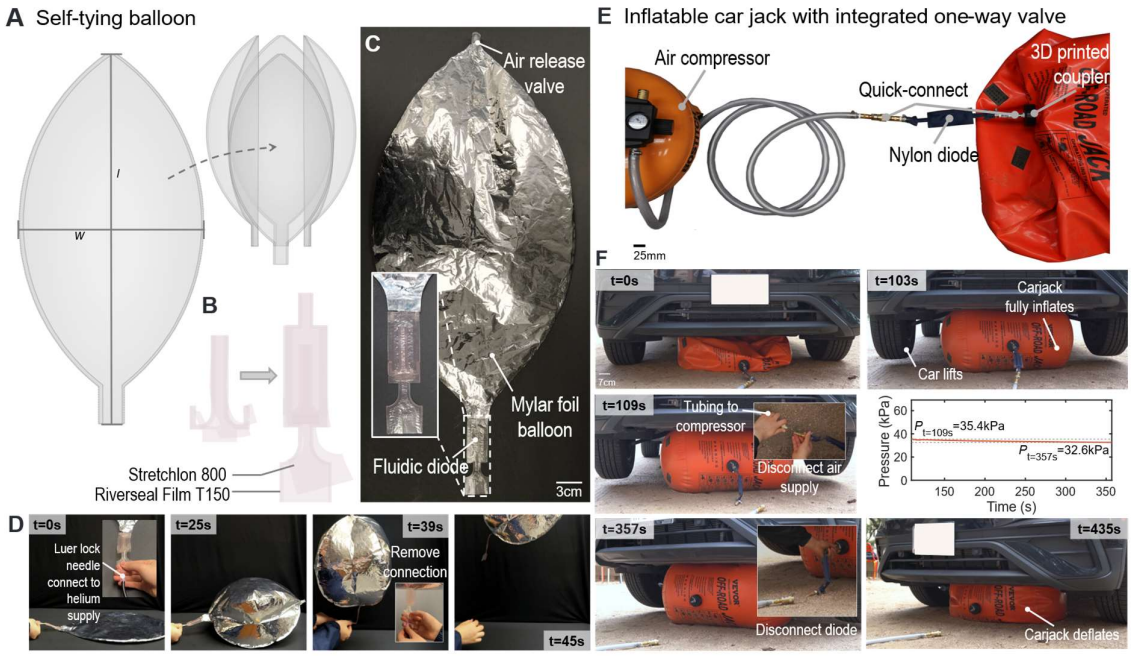

Figure 3. Two self-sealing devices. (A) Layers of a self-sealing mylar balloon, illustrating its assembly into a balloon using two-dimensional fabrication techniques. (B) The internal layout and layer assembly of the fluidic diode using thick nylon film as the substrate. Due to the high heat resistance of the nylon film (i.e., the layer melts and bonds at a higher temperature), the TPU acts as the adhesive layer that thermally bonds the two nylon layers. (C) Features of the modified balloon include a pressure-release valve and fluidic diode. (D) Operation of the balloon: We first filled the balloon with helium gas via a dispensing needle connected to a helium tank until it is full (by visually inspecting that the material appears taut, and the shape of the balloon is sufficiently round). Then, we shut off the helium supply and removed the needle from the inlet of the balloon. Next, we held the balloon for ~5 seconds, making sure not to pinch the inlet channel, and finally we let the balloon ascend. (E) Self-sealing inflatable car jack showing and an overview of the relevant components. (F) Operation of the car jack highlighting its ability to sustain a large, pressurized volume for a sufficient duration of time

to support the front axle of a 2022 Volkswagen Tiguan (~1750 kg). The pressure plot illustrates the loss of pressure starting when the air compressor is disconnected from the inlet of the diode to when the diode is disconnected from the coupler.

Self-sealing balloons offer a convenient solution to the challenges posed by the manual process of tying knots or using external ties and clips to seal balloons after inflation, a feature particularly useful for those with limited dexterity.[51,52] The self-sealing balloon developed in this work is fabricated by modifying a commercially-available mylar balloon with two additional features (**Figure 3**C): (i) a pressure-release valve at the tip of the balloon opposite to the filling port to allow for repeated use during experimental demonstrations (a component which would not be necessary during mass manufacturing or commercial use), and (ii) a fluidic diode attached at the inflating port used to supply gas (e.g., helium) into the balloon to provide a method of sealing after inflation that mitigates (but does not completely prevent) escape of helium from the balloon. In this demonstration, the fabrication of the fluidic diode involves two distinct material layers as illustrated in **Figure 3**B and uses a similar heat-sealing process as the fluidic diodes made from nylon taffeta characterized above. As for the layer assembly, we use nylon film as the substrate and a thick TPU film to thermally bond the layers; we select these materials for their low sheet density, thereby increasing the net buoyancy of the resulting balloon. As demonstrated in **Figure 3**D, we held the balloon for ~5 seconds after ceasing the supply of helium to the balloon; the observed behavior signifies that the inflated balloon experiences no substantial leakage. The balloon remained suspended in the air for more than one day.

Meanwhile, inflatable car jacks are valuable tools for lifting vehicles by providing a secure placement beneath various sections of the vehicle regardless of the terrain and are often compatible with portable air compressors (or even the pressure generated by a car's exhaust) to provide swift and efficient lifting support. Although offroad inflatable car jacks come with

exhaust jacks or filler tubes featuring integrated one-way valves, these components typically consist of inflexible and relatively heavy materials such as hard plastics or stainless steel, and they can fail or break if the car jack inflates in an incorrect configuration and presses them against the undercarriage. We investigated the potential of our sheet-based fluidic diode to achieve comparable prevention of backflow to valves included in standard car jack kits, highlighting its planar design consistent with the sheet-based structure of most inflatable car jacks, which can allow monolithic fabrication. Specifically, we retrofitted a commercially available inflatable car jack by affixing an adapter to the rubber interface of the filling port and linking an air compressor to the car jack using a fluidic diode fabricated from nylon taffeta. To initiate the lifting operation, we position the deflated car jack beneath the front of a vehicle and positioned the car jack sideways directly below the car's chassis. By gradually increasing the pressure of the air compressor from 0 to 410 kPa, we inflated the car jack until the front tires lifted off of the ground. After lowering the air supply to 0 kPa and disconnecting the coupler connecting to the compressor, the inflatable car jack remained inflated (**Figure 3**F), demonstrating proper sealing and thus the fluidic diode's ability to function with a high pressure differential and to withhold a substantial volume of compressed air for extended periods. Specifically, changing a tire typically takes on the order of minutes;[53] the loss of pressure within the car jack using our fluidic diode over ten minutes is only 12.7% (pressure within the car jack over a longer duration is provided in the Supplementary Information). Footage of the real-time demonstrations is shown in Supplementary Videos.

2.3. Fluidic Computing

2.3.1. Fundamental Logic Gates

By combining two fluidic diodes in parallel connected to serpentine-shaped fluidic resistors and pressure sources, we created diode logic gates capable of performing logical operations within soft robotic systems (**Figure 4**), opening possibilities for designing advanced fluidic systems capable of decision-making processes. The gates operate using pressure as Boolean logic levels where pressures are assigned to binary states. The compliance of the resulting device results in small fluctuations in the output pressure; however, the binary output pressure values (P) relative to the supply pressure (P_{SUPP}) remain within the range of $0.8 \leq P/P_{SUPP} \leq 1$ for a logical high ('1'), whereas a logical low ('0') corresponds to pressures close to atmospheric pressure, in the range of $0 \leq P/P_{SUPP} \leq 0.1$.

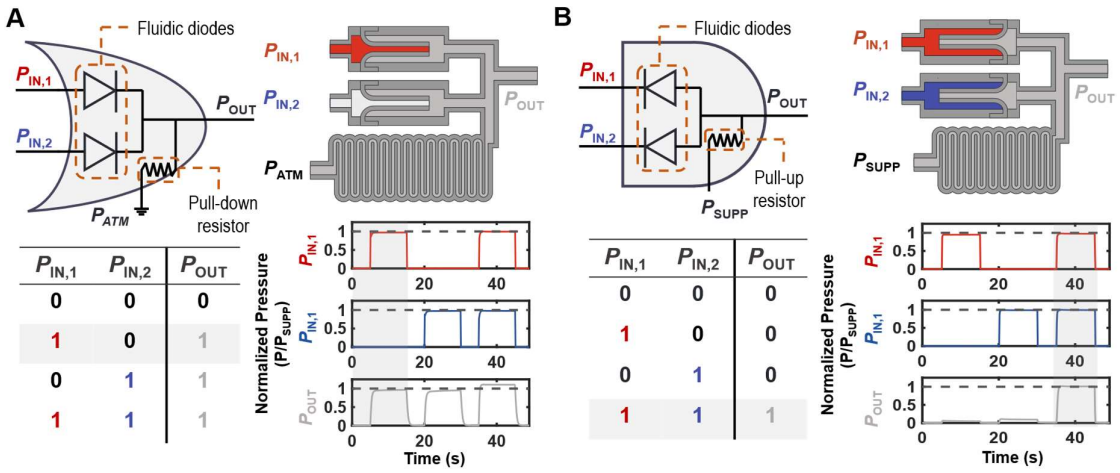

Figure 4. Digital control using pneumatic diode logic gates, where two fluidic diodes are configured in parallel. The placement of a serpentine-shaped fluidic resistor connected between the output and either P_{ATM} or P_{SUPP} allows realization of two fluidic logic gates: OR and AND, respectively. (A) An OR gate, configured by connecting the outlet junction of the diodes via a pull-down resistor to atmospheric pressure, with associated pressure traces plotted. (B) An AND gate, configured by connecting the outlet junction of the diodes via a pull-down resistor to the supply pressure, with associated pressure traces plotted. Each column of square waves represents the different input combinations and the resulting output states as represented in the corresponding truth table.

Each gate is configured to receive two inputs ($P_{IN,1}$, $P_{IN,2}$) corresponding to each of the two fluidic diodes, a reference pressure connected via a pull-down resistor to the junction of the

two diode outlets, and an output pressure at this junction (P_{OUT}). The OR gate outputs a logical high (‘1’) if either or both of the diodes are actuated (pressurized). In the OR gate, the forward flow of the diodes is connected to the output and the reference pressure is connected to the pneumatic ground (atmospheric pressure, P_{ATM}) via the pull-down resistor. The pull-down resistor ensures that the output state returns to a constant low pressure rather than remaining at the supply pressure P_{SUPP} when the inputs of the OR gate both reside at a low pressure (‘0’). For the AND gate, the forward flow is obtained from the inputs and the reference pressure is connected to a high-pressure supply (~0.4 bar, corresponding to binary ‘1’ in this case). With this configuration, the AND gate outputs a logical high (‘1’) if and only if the inlets of both diodes are actuated. For both logic gates, we use a thin serpentine path between sheets as the fluidic resistor; when pressurized, it approximates a length of tubing with a radius of ~0.55 mm (channel width of 1.75 mm for unpressurized state) to provide resistance to airflow. It is important to note that the logic gates were fabricated using nylon taffeta, and the design of the serpentine resistor may need to be modified accordingly if a different material were selected because the fluidic resistance is dependent, in part, on the bending behavior of the constituent material. To achieve a normalized pressure approaching ‘1’, the fluidic resistance of the pull-down resistor in the OR gate would need to approach infinity; in this limiting case, the response time for deflation would, however, also approach infinity (and thus result in slow switching speeds), presenting an important tradeoff in system design. Meanwhile, resistance of the pull-up resistor in the AND may be tuned such that the resistance is low enough to pull the output high within a suitable timeframe when both diodes are actuated but high enough to allow the output pressure to decrease to approximately atmospheric pressure (P_{ATM}) for all other cases.

Because logic gates are building blocks to more complex digital systems, the level to which logic gates may be cascaded—that is, combined in a sequential manner—is critical to allow

construction of useful logical operations. To build a logic circuit that tests the ability of logic gates to cascaded, the output of a given gate is routed as the input of the successive gate for any number of gates connected in series **(Figure 5**A-B**)**. To evaluate that the cascaded arrangement of the logic gates maintains logical consistency (i.e., negligible degradation of performance and functionality), we measured the forward signal propagation delay and the logic level drops. A low signal propagation delay is important for response times or how quickly the output reflects a change in input state and overall coordination of signals. **Figure 5**C-iii illustrates that each addition of a gate to a circuit results in an increased delay of < 0.1 seconds, comparable to the delay of other fluidic logic gates published in literature.[31,33,47] With the cascading gates, compounded fluidic resistance may cause significant pressure drops or a reduction in the signal amplitude, resulting in signal degradation. As indicated in **Figure 5**C-iv, the device experiences a logic pressure drop of < 2.5% per gate, indicating that additional gates do not significantly change the state of the signal when using approximately 4 gates in series or fewer, representing enough system complexity for memory storage, decision making, and more.[31–33]

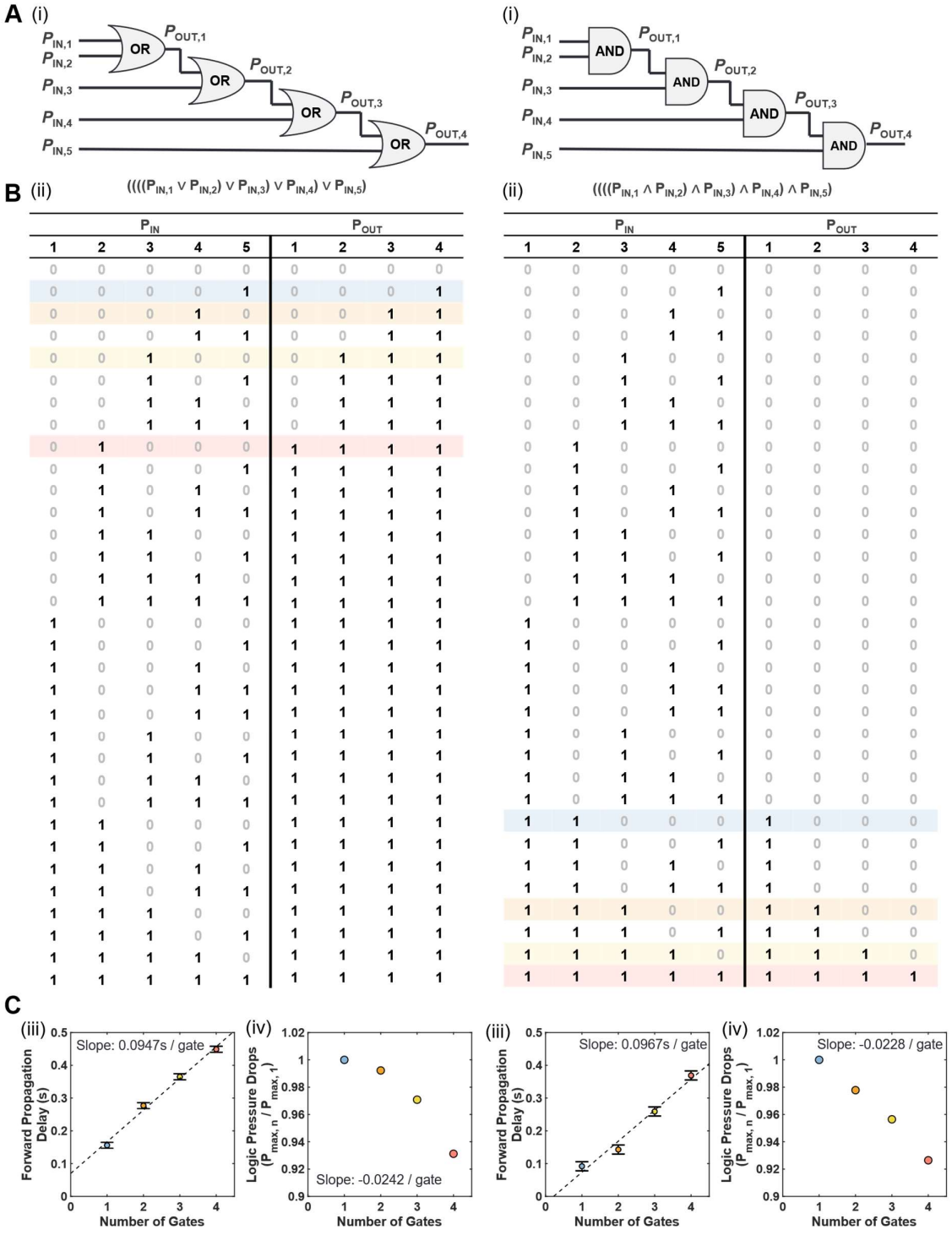

Figure 5. (A) Cascaded logic gates and the schematic diagram of the experimental setup used to measure the circuit performance. (B) Complete truth table of the cascaded logic gates for the corresponding logic circuits illustrated above. The highlighted rows of the truth table correspond to the configuration used to experimentally measure the delays and logic level drops with each added gate connected in series. (C-iii) The forward signal propagation delay as a function of the number of gate stages with OR gates (left) and AND gates (right). 100 individual measurements were averaged to obtain each of the datapoints. (C-iv) The logical

level drop where the highest pressure achieved from each additional stage is normalized by P_{HIGH} or the maximum pressure achieved output by a single logic gate.

2.3.2. Encoder using Diode Logic

Diodes can also be used for fluidic routing by directing fluid flow along designated pathways while preventing unwanted interactions between different input lines, ensuring that each input remains independent. To illustrate this principle, we created a fluidic encoder that outputs a 3-bit binary index for a single high (‘1’) input, enabling actuation of multiple output lines (or actuators) by activating a single input line. To direct the airflow through the device, we use pneumatic vias connecting the flow between the input layer with the configured diodes and the output layer connecting to pull-down resistors and pneumatic connections that exhaust the air to either the atmosphere or to connected actuator(s). Although binary logic relies on two distinct logic levels, provided that the input signals are driven by a large enough pressure signal, the exact magnitude of the pressure is not critical if the output signals lie within detectably varied pressure ranges. For an input of ~0.98 bar, the encoder outputs normalized pressure ranges of $0.8 \leq P/P_{IN} \leq 1$ for a logical high (‘1’) and a logical low (‘0’) between $0 \leq P/P_{IN} \leq 0.1$. Some pressure loss is expected given the increased fluidic resistance from interconnected channels and uneven pressure distribution between the pouches containing the diodes. We note that the serpentine pull-down resistors have not been optimized to decrease the system delay (i.e., the time taken for the device to fully transition from a high to low signal) or, inversely, the switching speeds as illustrated in **Figure 6**B–I with relatively shallow negative slopes of the falling edges observed in the measured pressure traces. Particularly, the resistance values should allow for the internal air to exhaust into the atmosphere while not creating an overly strong bias to ground when the input is high such that the output pressures lie within a reasonable pressure range.

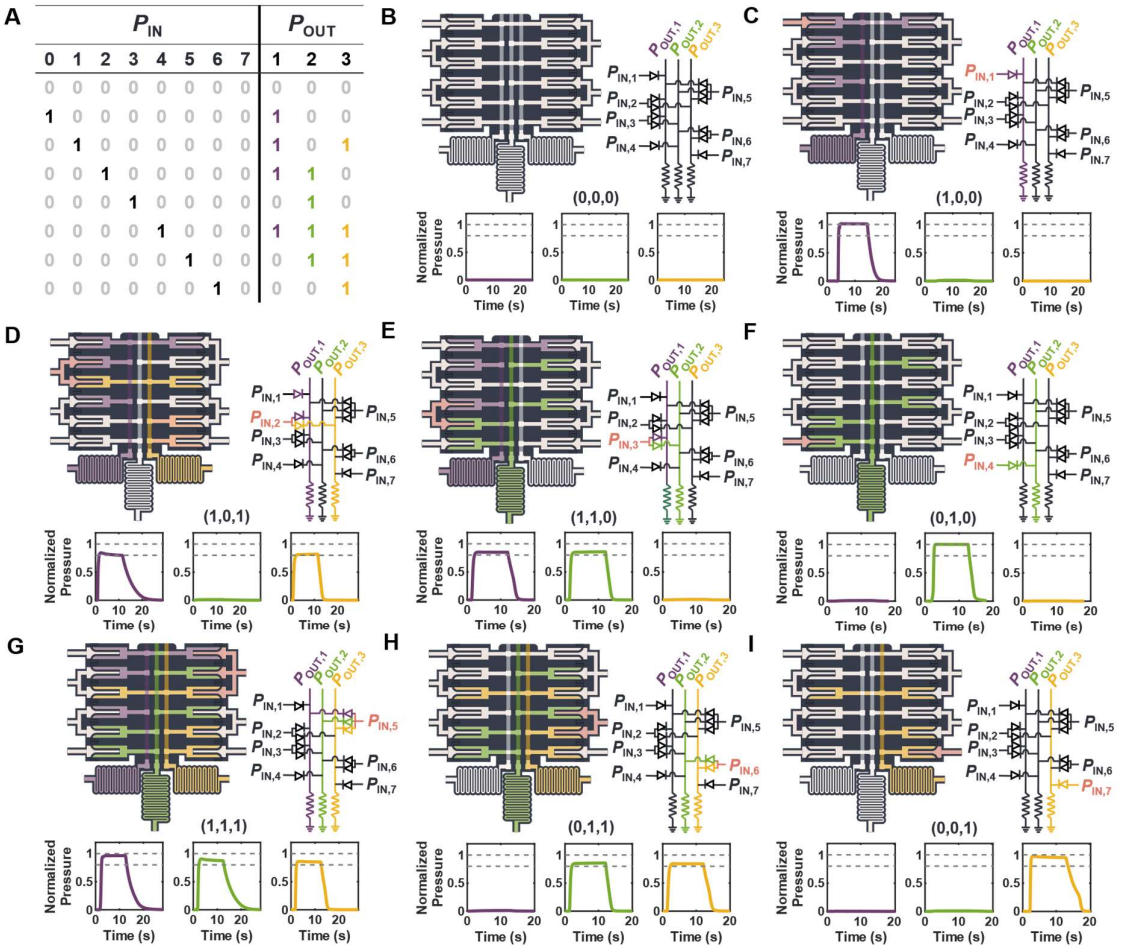

P_{IN}								P_{OUT}		
0	1	2	3	4	5	6	7	1	2	3
0	0	0	0	0	0	0	0	0	0	0
1	0	0	0	0	0	0	0	1	0	0
0	1	0	0	0	0	0	0	1	0	1
0	0	1	0	0	0	0	0	1	1	0
0	0	0	1	0	0	0	0	0	1	0
0	0	0	0	1	0	0	0	1	1	1
0	0	0	0	0	1	0	0	0	1	1
0	0	0	0	0	0	1	0	0	0	1

Figure 6. Fluidic encoder. (A) Full truth table of the encoder. (B-I) By designing the geometry and flow patterns using diodes as a method of isolating the multiple input lines, we created an encoder that maps 8 outputs to 3 inputs as illustrated in the plots of normalized pressure (P/P_{IN}) over time.

2.3.3. Diode Rectification

Another function of diodes is to rectify or control the flow direction during distinct phases of oscillation (i.e., to convert oscillatory fluidic input signals to direct current (DC)–like, positively phased constant fluidic signals). To demonstrate this capability, we integrate the fluidic diodes as check valves attached to a textile-based energy harvesting system based on a design reported in prior work.[49] The system uses an insole device composed of textile pouch filled with open-cell polyurethane foam that leverages its elasticity to draw atmospheric air into the pouch when the foot is lifted, but is compressed during foot strike which forces

pressurized air into a textile-based storage bladder to be used for powering pneumatic actuators. The original system relied on a pair of rigid plastic check valves to enforce unidirectional flow of air, where one valve prevents air from leaving the storage bladder during the insole's air intake phase (foot-off) and another valve prevents atmospheric air from leaving from the insole to atmosphere as it fills the bladder during the compression phase (foot-strike). For our modified system, we replace the downstream hard plastic check valve with our sheet-based fluidic diode fabricated from nylon taffeta—the same material used for the rest of the textile-based wearable system. As for the upstream hard plastic check valve, a fluidic diode cannot be substituted due to the lack of rigidity of the textile architecture. Specifically, the walls of the sheet-based diode collapse from the negative internal pressure relative to P_{ATM} resulting from the expansion of the foam to its original size following foot-off. To mitigate this issue, a hole is formed in the insole, allowing atmospheric air to enter at a faster rate. Without an additional diode, some air will escape from the insole during compression; nevertheless, the open-cell foam itself acts as a resistor with a higher value than the connected tubing on the bladder side, biasing the flow toward the channel connected to the diode and the bladder for storage of compressed air. We then conducted controlled experiments mimicking a person's walking gait by using two pneumatic pistons that switch at a period of 0.5 s (i.e., 2 steps per second, consistent with walking at 4.8 km/hr by adults age 30 and under).[54,55] Our experiment, illustrated in **Figure 7**A, simulates the oscillatory output of the walking cycle, where the positive phase corresponds to the actuation of the piston (i.e., application of foot-strike) which exerts a downward, compressive force on the textile insole that pushes the captured air to the pouch, and the negative phase corresponds to the release of the piston (i.e., foot-off) which allows the insole to expand and draw in atmospheric air. This conversion process reaches a steady state when the bladder achieves full inflation (**Figure 7**D). To simulate various body weights and associated heel forces on the insole pouches, we varied the input supply pressures to the pneumatic pistons with three different supply

pressures corresponding to F_{PISTON} that represent stepping forces of 196, 393, and 591 N (**Figure 7**C).

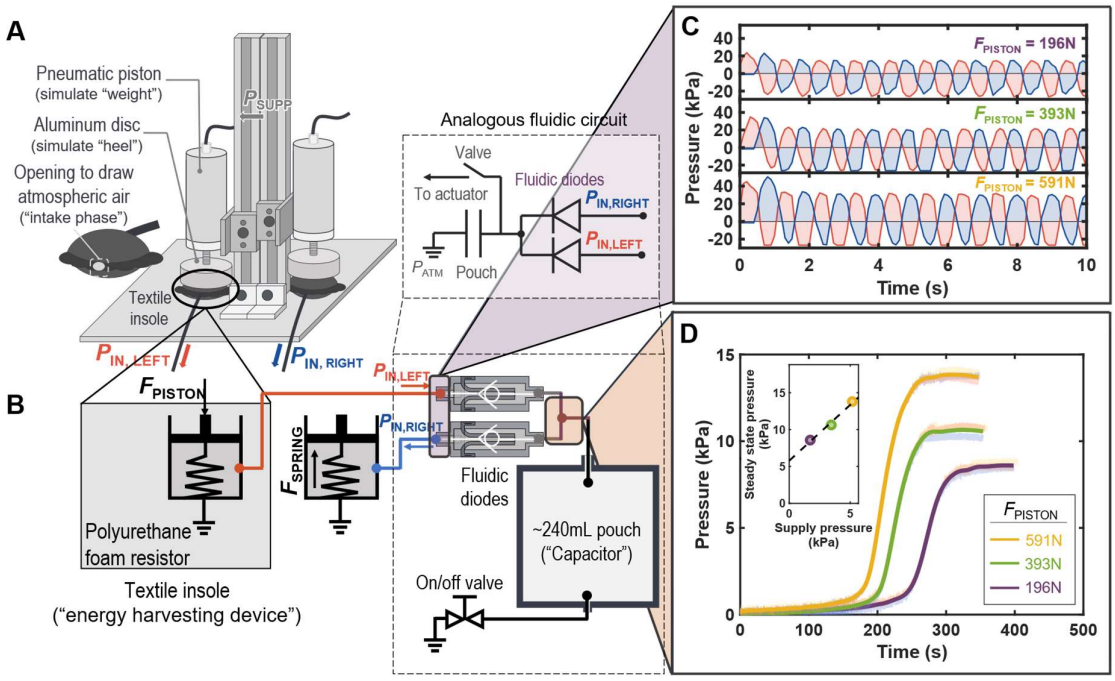

Figure 7. Experimental setup used to quantify performance of the diode rectifier for a textile-based energy harvesting system using the fluidic diode as a check valve. (A) Apparatus constructed to simulate walking in a controlled environment including the textile insole used to capture and accumulate the atmospheric air in the fluidic system. (B) Diagram of the pneumatic connections and direction of flow in the proposed energy harvesting system. (C) Sample output pressure traces obtained during the experiments illustrating the oscillatory inputs produced from the textile insoles. (D) The pouch's pressure as a function of time for various stepping forces averaged over three trials. The increase in the steady-state pressure output from the junction of the fluidic diodes as a function of the supply pressure (i.e., change in the maximum force pressing on the textile insole). The increasing slope shows an increase in the final pressure in the pouch (measured to fill ~240mL) as the supply pressure increases, for a given walking speed.

3. Conclusion

Onboard control schemes of pneumatically actuated soft robots have relied on electronic controllers and rigid, bulky electromechanical valves, imposing constraints on size and weight, which undermine the benefits of soft devices and systems where compliant and adaptive characteristics are desired or necessary. Soft fluidic devices provide an alternative approach to electronic controllers that can enable complex movements and incorporate feedback based on the environment or human users. This fluidic approach reduces the overall

complexity of the control systems required to generate and coordinate the actions of pneumatic actuators. Diodes remain an underutilized fluidic component with significant potential in mechanical computing. Soft, fluidic diodes have been underutilized because, as shown in prior work, they have exhibited at least one of two notable limitations: (i) they require a minimal closing pressure to completely restrict flow in the reverse direction, or (ii) they use hard materials to seal backflow or act as a physical barrier to block the flow passage, precluding seamless integration with planar or, broadly, sheet type soft robots and resulting in a bulky, non-compact design disadvantageous for applications within tight or constrained spaces that may require the full compliance expected of soft robots. To overcome these issues, we developed a fluidic diode fabricated from low-cost, flexible, sheet-based materials assembled in a layered thermal lamination process. The fluidic diode limits backflow through the passive self-pinching of a pneumatic channel connected to its inlet when the enclosing pouch of the diode is inflated. The fluidic resistance of sheet-based diodes in the forward direction is geometrically tunable to account for a range of pressures and operating conditions. Furthermore, we developed a scaling law where the fluidic resistance is inversely proportional to lengthscale to the third power, and the output flow rate is directionally proportional to that same internal fluidic resistance. Thus, increasing the size of the diode allows for higher rates of airflow. We note that the fabrication process constrains the dimensions of the fluidic diodes due to the cutting tolerances and bed sizes of commonly employed desktop fabrication devices. Additionally, the low bending stiffness of the sheet-based materials employed in this study means they are susceptible to kinking, and the mechanical properties of thin sheet materials utilized in our work may not possess desirable characteristics required for applications involving high actuating forces. Nevertheless, our experimental demonstrations show that the diodes can perform within pressure ranges (0–400 kPa) and flow rates typical for most pneumatic actuators and textile wearables .[48,56]

We leveraged the unidirectional flow enabled by the sheet-based diode to realize devices with self-sealing capabilities that maintain adequate levels of pressure for real-world use (exemplified in our construction of a self-sealing balloon and inflatable car jack). The diodes can also be configured to create fluidic computing elements, which are integrable in systems composed of compliant materials to regulate the flow of pressurized fluid. For example, we demonstrate the use of the diodes in digital fluidic logic, showcasing their capability of emulating the binary nature of digital systems by converting pneumatic inputs into digital signals or binary states defined by two distinct pressure ranges for control and computation. Specifically, we constructed logic gates that perform Boolean operations, OR and AND operators, allowing for simple, decision-making processes. Our diode logic gates, however, do not yield functionally complete digital logic systems because the output will always be the same phase as the input; consequently, the pneumatic signal cannot be inverted, and a NOT gate cannot be constructed. Fortunately, previous work has developed a sheet-based inverter (equivalent to a NOT gate) which can be combined with the diode logic gates shown here for a functionally complete set of logical connectives, leading to more complex logic functions.[31] Despite the lack of functional completeness when using diodes alone, in contrast to AND and OR gates using transistor-like elements (i.e., transistor-resistor logic), which require the use of three inverters,[31] the diode logic gates shown in this work use fewer fluidic elements and interconnections, offering a more compact approach. Furthermore, the tunable diode logic gates can be composed in a cascading manner with comparable performance to prior work, suggesting that diode logic gates can be used in a computing architecture in combination with other sheet-based fluidic analogs to electronic components. We also developed a 3-bit fluidic encoder composed entirely of diodes to map a single input to activate of a combination of output lines, enabling the actuation of multiple actuators. We also demonstrated the diodes' ability to respond to analog signals by using them as check valves in an energy harvesting system that converts oscillating input pressures to a positive-phased

output pressure that is then captured in a textile-based bladder acting as a pneumatic capacitor. It is important to note that fluidic systems exhibit substantially slower response speeds compared to their electronic counterparts due to the nature of information transport in fluid. Overall system volume, which is increased with additional tubing, valves, and other components to regulate the airflow, may also represent a limitation compared to electronic controllers. The durability of these systems, though, has been shown to surpass electronic counterparts in wearable applications,[31] and fluidic control is suitable for many low-level controllers, including in tandem with electronic systems.[30,57]

We envision our fluidic diodes as fundamental components in future development of sheet-based logic controllers, including embedded textile-logic systems for soft wearables and pneumatic assistive devices or soft robots with on-demand collapsibility for ease of deployment, like origami-inspired soft robots. The two-dimensional architecture of these diodes also allows them to be combined with other sheet-based fluidic devices in a monolithic architecture to create modular, advanced integrated circuits (ICs)—with ultimate aims to create computing devices, actuators, and sensing components that can directly interface with each other to build integrated soft robotic systems that are programmable and reactive to the environment.

4. Experimental Section/Methods

Fabrication of Textile Fluidic Diode and Logic Devices: To fabricate the fluidic diode and logic devices, we applied an adhesive paper tape (V0821, Vinyl Ease) to mask the TPU-coated side of heat-sealable nylon taffeta fabric (Riverseal 70 LW, Rivertex Technical Fabrics Group). We then patterned the masked side using a desktop vinyl cutter (Maker, Cricut) that forms the internal geometries and pathways for airflow within the device; the outlines of the paper mask were engraved using the "Washi Tape" setting at "low pressure" while cuts through the textile layer were made using "Copy Paper" setting at "high pressure." After weeding the extraneous areas of the mask, the layers were stacked, vertically aligned, and thermally bonded using a benchtop heat press (DK20SP, Geo Knight & Co Inc.) at 180° C and 35 kPa platen pressure for a duration of 30 s. We recommend pressing the device as it cools to ensure a strong bond of the heat-sealable textiles and prevent wrinkles. Finally, pneumatic ports (stainless steel dispensing needle with Luer lock connection; 75165A272, McMaster-Carr) were attached to the heat-sealed device using two-part epoxy glue (clear epoxy, Gorilla Inc.) to create airtight joints. Pneumatic connections between the pressure supply source and pneumatic polyurethane connections were all wired using flexible polyurethane tubing (3/32" inside diameter; 5648K231, McMaster-Carr). Detailed instructions on the fabrication and assembly of each device is outlined in the Supplementary Materials.

Characterization and Pneumatic Testing of Fluidic Devices: The pressure inputs of the fluidic diodes and logic devices were supplied from compressed air line fed to a pressure regulating valve (PR364, Parker Hannifin Corporation). The input of the diode was connected to the compressed air supply and the input pressure was linearly increased from 0 kPa at intervals of 50 kPa until a flow rate of approximately 5 L min^{-1} is achieved, the maximum rated flow rate

of the connecting flowmeter at the outlet of the diode. With each interval, we obtain the static pressure measurements at steady state using digital pneumatic pressure gauges (MG1-30-A-9V-R, SSI Technologies Inc.). For transient measurements, such as the logic gates and rectifier, input and output pressure signals were measured using electronic pressure sensors (ADP5151, Panasonic Corporation) connected to an analog voltage acquisition device (USB-6002, National Instruments). For logic gates, we generate the square-wave input signals by first setting the supply pressure with a manual pressure regulator at 40 kPa and then splitting the lines through pneumatic solenoid valves (VT307-5DZ1-02N-F) using a tee connector (51525K445, McMaster-Carr) connected at the inlet of each diode. As for the reference pressures connected to the resistors, the port of the OR gate is open to atmospheric air for a pull-down resistor and the port of the AND gate is connected to the supply pressure line using another tee connector. The valve was then switched between the supply and exhaust pressures using pulsed digital output from a data acquisition device (USB-6210, National Instruments). Each combination of inputs represented in the truth table was demonstrated by supplying an input signal for 10s with a 5s pause in-between to allow the system to reset (i.e., exhaust pressurized air in the device to atmosphere). For the encoder, each of the seven inputs were connected to a 100-kPa compressed air supply that is switched on and off by a single-action air directional control valve (62475K14, McMaster-Carr) connected to a manifold (5469K101, McMaster-Carr). The square-wave inputs were timed for a period of approximately 10 s. Pressure traces were recorded from the data acquisition device interfaced to a computer, and the collected data was processed using custom scripts in Matlab (version R2022a, MathWorks Inc.).

Fabrication and Testing of Self-Sealing Balloon: For fabrication of the self-sealing balloon, we modified an existing mylar balloon (B098FC99FM, KatchOn) by cutting a section of the top to epoxy a plastic tube plug (51525K271, McMaster-Carr) connected to a plastic cap

(51525K245, McMaster-Carr) to exhaust the helium and the bottom to insert the diode valve. To create the sheet diode, we used similar technique of vector cutting and stacked heat sealing where the perimeter of the device is cut from thin TPU film (Stretchlon 800, Airtech International Inc.) and the internal volumes of the device are defined by sealing layers with a thicker TPU film (Riverseal Film T150 87A, Rivertex Technical Fabrics Group) to create an airtight seal around the edges. The geometry of the inlet of the nylon fluidic diode in the forward direction is designed to be retrofitted to the nozzle of the helium tank (B01M0PG5BD, BalloonTime). For the testing of the balloon, we attached a flexible polyurethane tube (6516T62, McMaster-Carr) connected to a Luer lock connection (51525K12, McMaster-Carr) with a dispensing needle (75165A249, McMaster-Carr) that is then inserted into the inlet of the flexible diode. Helium is released to the balloon from the tank by compressing the nozzle. Once inflated, the balloon can be deflated by disconnecting the plastic cap to exhaust the helium to the environment.

Modification of Inflatable Car Jack: For the demonstration, we attached a custom adapter to the inlet of a commercially available inflatable car jack (B092ML7TMC, Wayska) with the hexagonal end of the barbed tube fitting epoxied to the open center (5058K826, McMaster-Carr). The fitting was then connected to a quick-disconnect coupling (¼-in NPT and ⅜-in Pipe Size; 5602K25, McMaster-Carr) connected to the fluidic diode fabricated from nylon taffeta and connected to another quick-disconnect coupling (¼ NPT and ⅜ Pipe Size; 6534K27 and 1077T18, McMaster-Carr). The inlets of the diodes were further reinforced by epoxying 1” long PVC plastic tubing (⅜” ID; 5238K748, McMaster-Carr) to prevent kinking during inflation and connection of the tube to the textile was further clamped using hose clamps (5415K15, McMaster-Carr). The adapter was 3D printed using a fused-deposition modeling (FDM) printer (Creality CR-10S Pro) and G-code was generated using slicing software with parameters and printing settings following standard quality (0.8-mm wall

thickness, printing temperature of 215° C and build plate temperature of 60° C). To inflate, we initially supplied the car jack with 20 psi and slowly increased the pressure to 60 psi via an air compressor (B00UHNM1R0, Bostitch) with the given hose connected to the adapter.

Experimental Setup and Pneumatic Testing of Diode Rectification: The textile insoles were fabricated with pouch volume of approximately 35 mL following similar fabrication methods outlined in the work of a wearable textile-based pneumatic energy harvesting system.[58] The design of the textile is modified with an additional port which allows a small opening where the foam is exposed to the atmosphere to circumvent the negative pressure problem described earlier in this work, and the another port is connected to flexible rubber tubing (9776TI, McMaster-Carr) with pneumatic connectors. To create the apparatus that will simulate the walking gate, we assembled a mechanofluidic system that uses round-body air cylinders (1-1/2" Bore, 1" Stroke; 6498K211, McMaster-Carr) that are actuated by supplying the lab's compressed air at three different pressures to represent the different magnitudes of step forces varied by a person's weight: 25 kPa, 50k Pa, and 75 kPa. The air cylinders are secured to T-slotted frames which are then secured to a plate with brackets. The ends of the cylinders have aluminum disk contact pads that represent the area of the heel when pressed upon the textile insole pouches (2-in diameter; 1610T15, McMaster-Carr). A hole is tapped into the aluminum using a steel general purpose tap (1-7/16-in thread length, McMaster-Carr) allowing the aluminum plate to be screwed to the nose of the air cylinders. The periodic compression and release of the textile insoles were controlled by oscillatory square-wave pressure signals generated by solenoid valves controlled by an electronic computer as previously described.

Supporting Information

Supporting Information is available from the Wiley Online Library or from the author.

Acknowledgements

V.T.V. acknowledges support from the Rice Undergraduate Scholar Program and Rice University Research Experience for Undergraduates. A.R. acknowledges support from the Rice University Academy of Fellows. B.J. acknowledges support from the National Science Foundation (NSF) Graduate Research Fellowship under Grant No. 1842494. Any opinions, findings, and conclusions or recommendations expressed in this material are those of the authors and do not necessarily reflect the views of the NSF. M.D.B. recognizes support from a NASA Space Technology Graduate Research Opportunity award (80NSSC21K1276) and a National GEM Consortium Fellowship. This work was supported by the NSF under Grant No. CBET-2030023.

Received: ((will be filled in by the editorial staff))

Revised: ((will be filled in by the editorial staff))

Published online: ((will be filled in by the editorial staff))

References

[1] B. Jumet, M. D. Bell, V. Sanchez, D. J. Preston, *Adv. Intell. Syst.* **2022**, *4*, 2100163.
[2] C. Lee, M. Kim, Y. J. Kim, N. Hong, S. Ryu, H. J. Kim, S. Kim, *Int. J. Control Autom. Syst.* **2017**, *15*, 3.
[3] G. M. Whitesides, *Angew. Chem. Int. Ed.* **2018**, *57*, 4258.
[4] S. Kim, C. Laschi, B. Trimmer, *Trends Biotechnol.* **2013**, *31*, 287.
[5] P. Polygerinos, N. Correll, S. A. Morin, B. Mosadegh, C. D. Onal, K. Petersen, M. Cianchetti, M. T. Tolley, R. F. Shepherd, *Adv. Eng. Mater.* **2017**, *19*, 1700016.
[6] S. I. Rich, R. J. Wood, C. Majidi, *Nat. Electron.* **2018**, *1*, 102.
[7] A. Rajappan, B. Jumet, D. J. Preston, *Sci. Robot.* **2021**, *6*, eabg6994.
[8] C. Christianson, C. Bayag, G. Li, S. Jadhav, A. Giri, C. Agba, T. Li, M. T. Tolley, *Front. Robot. AI* **2019**, *6*, 126.
[9] Y. Matia, G. H. Kaiser, R. F. Shepherd, A. D. Gat, N. Lazarus, K. H. Petersen, *Adv. Intell. Syst.* **2023**, *5*, 2200330.
[10] K. McDonald, A. Rendos, S. Woodman, K. A. Brown, T. Ranzani, *Adv. Intell. Syst.* **2020**, *2*, 2000139.
[11] M. Wehner, R. L. Truby, D. J. Fitzgerald, B. Mosadegh, G. M. Whitesides, J. A. Lewis, R. J. Wood, *nature* **2016**, *536*, 451.
[12] B. Mosadegh, P. Polygerinos, C. Keplinger, S. Wennstedt, R. F. Shepherd, U. Gupta, J. Shim, K. Bertoldi, C. J. Walsh, G. M. Whitesides, *Adv. Funct. Mater.* **2014**, *24*, 2163.
[13] N. Vasios, A. J. Gross, S. Soifer, J. T. Overvelde, K. Bertoldi, *Soft Robot.* **2020**, *7*, 1.

[14] D. Drotman, S. Jadhav, D. Sharp, C. Chan, M. T. Tolley, *Sci. Robot.* **2021**, *6*, eaay2627.
[15] M. Wehner, R. L. Truby, D. J. Fitzgerald, B. Mosadegh, G. M. Whitesides, J. A. Lewis, R. J. Wood, *nature* **2016**, *536*, 451.
[16] C. J. Decker, H. J. Jiang, M. P. Nemitz, S. E. Root, A. Rajappan, J. T. Alvarez, J. Tracz, L. Wille, D. J. Preston, G. M. Whitesides, *Proc. Natl. Acad. Sci.* **2022**, *119*, e2205922119.
[17] J. Wang, A. Chortos, *Adv. Intell. Syst.* **2022**, *4*, 2100165.
[18] J. D. Hubbard, R. Acevedo, K. M. Edwards, A. T. Alsharhan, Z. Wen, J. Landry, K. Wang, S. Schaffer, R. D. Sochol, *Sci. Adv.* **2021**, *7*, eabe5257.
[19] M. Calisti, G. Picardi, C. Laschi, *J. R. Soc. Interface* **2017**, *14*, 20170101.
[20] K. McDonald, T. Ranzani, *Front. Robot. AI* **2021**, 266.
[21] M. Adams, M. Johnston, A. Scherer, S. Quake, *J. Micromechanics Microengineering* **2005**, *15*, 1517.
[22] J. Liu, Y. Chen, C. R. Taylor, A. Scherer, E. P. Kartalov, *J. Appl. Phys.* **2009**, *106*, 114311.
[23] K. Hosokawa, R. Maeda, *J. Micromechanics Microengineering* **2000**, *10*, 415.
[24] M. A. Unger, H.-P. Chou, T. Thorsen, A. Scherer, S. R. Quake, *science* **2000**, *288*, 113.
[25] V. Magdanz, S. Sanchez, O. G. Schmidt, *Adv. Mater.* **2013**, *25*, 6581.
[26] A. K. Au, W. Huynh, L. F. Horowitz, A. Folch, *Angew. Chem. Int. Ed.* **2016**, *55*, 3862.
[27] P. N. Duncan, T. V. Nguyen, E. E. Hui, *Proc. Natl. Acad. Sci.* **2013**, *110*, 18104.
[28] B. Mosadegh, C.-H. Kuo, Y.-C. Tung, Y. Torisawa, T. Bersano-Begey, H. Tavana, S. Takayama, *Nat. Phys.* **2010**, *6*, 433.
[29] Q. Zhang, M. Zhang, L. Djeghlaf, J. Bataille, J. Gamby, A. Haghiri-Gosnet, A. Pallandre, *Electrophoresis* **2017**, *38*, 953.
[30] W.-K. Lee, D. J. Preston, M. P. Nemitz, A. Nagarkar, A. K. MacKeith, B. Gorissen, N. Vasios, V. Sanchez, K. Bertoldi, L. Mahadevan, *Sci. Robot.* **2022**, *7*, eabg5812.
[31] A. Rajappan, B. Jumet, R. A. Shveda, C. J. Decker, Z. Liu, T. F. Yap, V. Sanchez, D. J. Preston, *Proc. Natl. Acad. Sci.* **2022**, *119*, e2202118119.
[32] D. J. Preston, H. J. Jiang, V. Sanchez, P. Rothemund, J. Rawson, M. P. Nemitz, W.-K. Lee, Z. Suo, C. J. Walsh, G. M. Whitesides, *Sci. Robot.* **2019**, *4*, eaaw5496.
[33] D. J. Preston, P. Rothemund, H. J. Jiang, M. P. Nemitz, J. Rawson, Z. Suo, G. M. Whitesides, *Proc. Natl. Acad. Sci.* **2019**, *116*, 7750.
[34] P. Rothemund, A. Ainla, L. Belding, D. J. Preston, S. Kurihara, Z. Suo, G. M. Whitesides, *Sci. Robot.* **2018**, *3*, eaar7986.
[35] K. Luo, P. Rothemund, G. M. Whitesides, Z. Suo, *J. Mech. Phys. Solids* **2019**, *131*, 230.
[36] J. A. Tracz, L. Wille, D. Pathiraja, S. V. Kendre, R. Pfisterer, E. Turett, C. K. Abrahamsson, S. E. Root, W.-K. Lee, D. J. Preston, *IEEE Robot. Autom. Lett.* **2022**, *7*, 5483.
[37] A. Davletshin, T. C. Underwood, W. Song, *Adv. Funct. Mater.* **2022**, *32*, 2200658.
[38] Q. Lu, H. Xu, Y. Guo, J. Y. Wang, L. Yao, **2023**, pp. 1–21.
[39] N. Napp, B. Araki, M. T. Tolley, R. Nagpal, R. J. Wood, IEEE, **2014**, pp. 1440–1445.
[40] J. Li, H. Jia, J. Zhou, X. Huang, L. Xu, S. Jia, Z. Gao, K. Yao, D. Li, B. Zhang, *Nat. Commun.* **2023**, *14*, 5009.
[41] D. P. Holland, C. Abah, M. Velasco-Enriquez, M. Herman, G. J. Bennett, E. A. Vela, C. J. Walsh, *IEEE Robot. Autom. Mag.* **2017**, *24*, 57.
[42] H. Philamore, I. Ieropoulos, A. Stinchcombe, J. Rossiter, *Soft Robot.* **2016**, *3*, 186.
[43] S. Wu, Q. Ze, J. Dai, N. Udipi, G. H. Paulino, R. Zhao, *Proc. Natl. Acad. Sci.* **2021**, *118*, e2110023118.
[44] Q. Ze, S. Wu, J. Dai, S. Leanza, G. Ikeda, P. C. Yang, G. Iaccarino, R. R. Zhao, *Nat. Commun.* **2022**, *13*, 3118.
[45] Z. Chen, B. Tighe, J. Zhao, *IEEEASME Trans. Mechatron.* **2022**, *27*, 2016.

[46] D. Rus, M. T. Tolley, *Nat. Rev. Mater.* **2018**, *3*, 101.
[47] W. Yan, S. Li, M. Deguchi, Z. Zheng, D. Rus, A. Mehta, *Nat. Commun.* **2023**, *14*, 1553.
[48] V. Sanchez, C. J. Walsh, R. J. Wood, *Adv. Funct. Mater.* **2021**, *31*, 2008278.
[49] N. Persson, J. G. Martinez, Y. Zhong, A. Maziz, E. W. Jager, *Adv. Mater. Technol.* **2018**, *3*, 1700397.
[50] C. Thalman, P. Artemiadis, *Wearable Technol.* **2020**, *1*, e3.
[51] Z. A. RASTI, A. Shamsoddini, H. Dalvand, S. Labaf, *Iran. J. Child Neurol.* **2017**, *11*, 43.
[52] S. B. Tajali, J. C. MacDermid, R. Grewal, C. Young, *Open Orthop. J.* **2016**, *10*, 190.
[53] M. A. Sharp, B. S. Cohen, M. W. Boye, S. A. Foulis, J. E. Redmond, K. Larcom, J. R. Hydren, D. L. Gebhardt, M. C. Canino, B. J. Warr, *J. Sci. Med. Sport* **2017**, *20*, S62.
[54] M. Schimpl, C. Moore, C. Lederer, A. Neuhaus, J. Sambrook, J. Danesh, W. Ouwehand, M. Daumer, *PloS One* **2011**, *6*, e23299.
[55] C. Tudor-Locke, H. Han, E. J. Aguiar, T. V. Barreira, J. M. Schuna Jr, M. Kang, D. A. Rowe, *Br. J. Sports Med.* **2018**, *52*, 776.
[56] P. Boyraz, G. Runge, A. Raatz, MDPI, **2018**, p. 48.
[57] B. Jumet, Z. A. Zook, A. Yousaf, A. Rajappan, D. Xu, T. F. Yap, N. Fino, Z. Liu, M. K. O'Malley, D. J. Preston, *Device* **2023**, *1*.
[58] R. A. Shveda, A. Rajappan, T. F. Yap, Z. Liu, M. D. Bell, B. Jumet, V. Sanchez, D. J. Preston, *Sci. Adv.* **2022**, *8*, eabo2418.
[59] V. Sanchez, C. J. Walsh, R. J. Wood, *Adv. Funct. Mater.* **2021**, *31*, 2008278.

Journal's Table of Contents (ToC)

Sheet-Based Fluidic Diodes for Embedded Fluidic Circuitry in Soft Devices

Vi T. Vo, Anoop Rajappan, Barclay Jumet, Marquise D. Bell, Sofia Urbina, Daniel J. Preston

V. T. Vo, Dr. A. Rajappan, B. Jumet, M. D. Bell, S. Urbina, Prof. D. J. Preston

Department of Mechanical Engineering, Rice University, Houston, TX 77005, USA

E-mail: djp@rice.edu

ToC Text

To reduce the demand for electromechanical valves and electronic controllers within soft robots and to simplify the actuation of multi-pressure systems, this work presents sheet-based fluidic diodes fabricated from flexible polymer sheets and textiles using a layered fabrication approach. These diodes leverage their unidirectional flow to enable electronics-free soft devices capable of performing digital logic operations, encoding, and rectification.

ToC Figure